Phonon excitations in $Eu_2Ir_2O_7$ probed by inelastic X-ray scattering

Han Wang[1], R. Kaneko[2,3], Y. Zhang[4], A. Baron[5], D. Ishikawa[5], B. Wehinger[6], E. Dagotto[4,7], Y. Tokura[2,3,8], T.-H Arima[2,7], K. Ueda[2,3*], S. Gao[1,2†]

[1]Department of Physics, University of Science and Technology of China, Hefei 230026, China
[2]RIKEN Center for Emergent Matter Science, Wako 351-0198, Japan
[3]Department of Applied Physics, University of Tokyo, Tokyo 113-8656, Japan
[4]Department of Physics and Astronomy, University of Tennessee, Knoxville, 37996, USA
[5]Materials Dynamics Laboratory, RIKEN SPring-8 Center, Sayo 679-5198, Japan
[6]European Synchrotron Radiation Facility, 71, Avenue des Martyrs, Grenoble 38000, France
[7]Materials Science and Technology Division, Oak Ridge National Laboratory, Oak Ridge 37831, USA
[8]Tokyo College, University of Tokyo, Tokyo 113-8656, Japan
[9]Department of Advanced Materials Science, University of Tokyo, Kashiwa 277-8561, Japan

E-mail: * `ueda@ap.t.u-tokyo.ac.jp`, † `sgao@ustc.edu.cn`

Abstract.
 The study of phonon dynamics and its interplay with magnetic ordering is crucial for the understanding the unique quantum phases in the pyrochlore iridates. Here, through inelastic X-ray scattering on a single crystal sample of the pyrochlore iridate $Eu_2Ir_2O_7$, we map out the phonon excitation spectra in $Eu_2Ir_2O_7$ and compare them with the theoretical phonon spectra calculated using the density functional theory. Possible phonon renormalization across the magnetic long-range order transition is revealed from the temperature dependence of the phonon spectra.

Submitted to: *J. Phys.: Condens. Matter*

1. Introduction

The explorations of the $4d$ and $5d$ heavy transitional metal electronic systems represent a cutting-edge research domain in condensed matter physics. These systems harbor a plethora of unconventional correlated states, including quantum spin liquids [1, 2, 3], metal-insulator transitions [4, 5], Weyl semimetals (WSM) [6], topological insulators [7, 8], non-Fermi liquids [9], magnetic monopole-like phase [10], etc. The intriguing manifestations of these states arise from a unique amalgamation of factors, including extended $5d/4d$ orbitals [11], strong spin-orbit coupling (SOC), and geometrically frustrated lattices [12], thus offering a rich platform to search for exotic correlated states.

Among the heavy transitional metal electron systems, the pyrochlore iridates, R_2Ir$_2$O$_7$ (R = Y and rare earth ions) [13, 14, 15, 16, 17], stand out as a fertile ground to realize novel quantum states. The structure of the pyrochlore iridates is presented in Fig. 1(a), where the Ir^{4+} ions form a pyrochlore lattice with corner-sharing tetrahedra. The Ir^{4+} ions of the low-spin configuration form an effective doublet of J = 1/2, where J is the total angular momentum [18]. For compounds with a relatively large R^{3+} ion radius, a metal-insulator transition (MIT) has been observed, where the transition temperature, T_N, can be tuned by various external parameters including chemical composition [19, 20, 21], pressure [22, 23, 24], and magnetic field [25, 26, 27, 28]. In the insulating phase, the magnetic moments of the Ir^{4+} ions form an 'all-in/all-out' (AIAO) magnetic long range-order, which can be viewed as a solidified phase of magnetic monopoles [29]. For compounds with a relatively small R^{3+} ion radius, the paramagnetic phase at temperatures above the ordering transition become insulating, indicating a strong correlation between the chemical pressure and electronic bands [30].

The lattice degree of freedom of the pyrochlore iridates also contains rich information about the spin correlations because the lattice is directly connected to the orbitals and, consequently, indirectly influences the spins through SOC [31]. Recent Raman scattering experiments on Eu$_2$Ir$_2$O$_7$ revealed significant renormalization of the phonon frequencies across $T_N \sim 115$ K [32]. Furthermore, the noncollinear character of the AIAO structure allows a linear coupling between the magnons and phonons, meaning that hybridized spin-lattice excitations may emerge if the exchange couplings between the Ir^{4+} spins depend on their distances [32, 33].

In this work, we performed non-resonant inelastic X-ray scattering (IXS) experiments to map out the phonon dispersion in Eu$_2$Ir$_2$O$_7$ and compare it to the theoretical spectra calculated by the first-principle density functional theory (DFT). Possible phonon
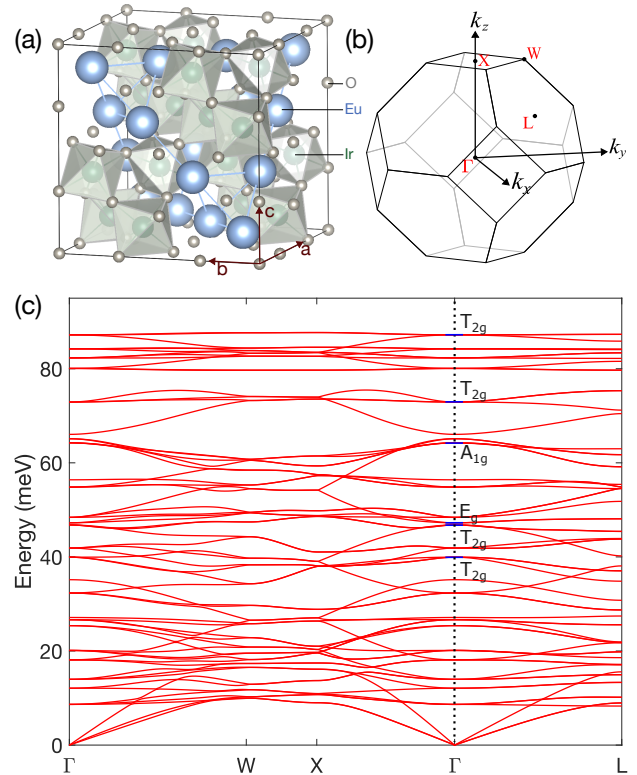
Figure 1. (a) Crystal structure of the pyrochlore iridates. The large blue sphere is the Eu site. The large green sphere with polyhedra is Ir. The small grey one is O. (b) Brillouin zone and high symmetry points for the face-centered cubic (FCC) lattice. (c) DFT calculations of the phonon dispersion along the high-symmetry directions Γ-W-X-Γ-L.

renormalization across T_N is observed at selected wave vector transfers near the Brillouin zone center, although hybrid magnon-phonon excitations are not resolved in our experiments possibly due to their relatively low scattering cross sections.

2. Methods

Our IXS experiments were performed on the RIKEN Quantum NanoDynamics Beamline, BL43LXU [34], at the SPring-8 synchrotron light source in Japan. This beamline provides world-leading intensity for IXS experiments using 3×5 m insertion devices [35, 36] in a small, 50 µm diameter beam spot. A piece of KF-flux grown Eu$_2$Ir$_2$O$_7$ single crystal [37], with a dimension of $0.4 \times 0.4 \times 0.1$ mm^3, was used for the experiments. The reflection scattering geometry was employed due to the relatively short attenuation length of ~ 20 µm at an incoming x-ray energy of 20 keV. The (111) surface of the crystal was polished and vertically attached to the sample holder, which was then aligned with the (HHL) plane horizontally. The 24 analyzer array allows parallel measurements over a large area of momentum transfers. The Si (11,11,11) setup with a

resolution of > 1.3 meV (depending on analyzer) was employed. A closed cycle cryostat was mounted in the Eulerian cradle to access temperatures down to ~ 50 K. The IXS energy scale is expected to be accurate to 0.5 % based on calibration against a standard [38].

Theoretical phonon spectra for $Eu_2Ir_2O_7$ at zero temperature were calculated using the first-principles density functional theory (DFT) as implemented in the Vienna *ab initio* simulation package (VASP). The projector augmented wave (PAW) method with the generalized gradient approximation (GGA) and the Perdew-Burke-Ernzerhof (PBE) exchange potentials were employed [39, 40, 41, 42]. The Debye Waller factor was not considered in our calculations. The plane-wave cutoff energy was set as 600 eV and the k-point mesh was set as $6 \times 6 \times 6$ for the conventional cell of the cubic $Fd\bar{3}m$ phase (No. 227) of $Eu_2Ir_2O_7$. For the structural optimization in the paramagnetic phase, the lattice constant was fixed at the experimental value of $a = 10.167$ Å, and the atomic positions were fully relaxed until the Hellman-Feynman force on each atom was smaller than 0.001 eV/Å. Force constants were calculated by density functional perturbation theory [43, 44] as implemented in VASP. Phonon dispersion relations were obtained using the PHONONPY software in a primitive unit cell [45, 46].

3. Results and Discussions

Figure 1 presents an overview of the calculated phonon dispersion along the high symmetry lines in reciprocal space. The absence of imaginary frequencies corroborates the accuracy of our structural optimization. Altogether 66 phonon bands are observed in our calculations, which is consistent with the number of phonon modes for 22 atoms per primary unit cell. At the Brillouin zone center, i.e. the Γ point, there are 6 Raman-active phonon bands according to group-theoretical analysis [32]:

$$\Gamma^{op} = A_{1g} + E_g + 4T_{2g}. \qquad (1)$$

These Raman active modes are indicated in Fig. 1(c). As compared in Tables 1 and 2 for the Raman- and infrared-active modes, respectively, our calculated frequencies are in good agreement with the previous DFT calculations and the experimental observations at $T = 300$ K [32]. For the E_g mode that is the focus of our present study, the calculated and experimental energies are 47.2 and 41.8 meV, respectively. This slightly overestimated energy may arise from the coupling between phonons and low-energy excitations of the valence electrons [32], which is not included in DFT calculations.

Figure 2 compares the experimental and calculated IXS cross sections along the $(66L)$ and $(HH8)$
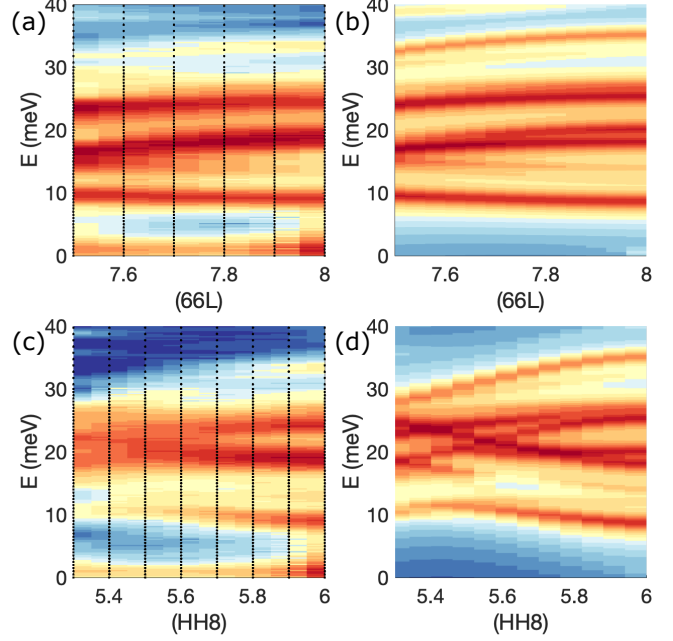
Figure 2. (a) Experimental and (b) calculated phonon IXS spectra along the $(66L)$ r.l.u. direction. The experimental data are collected at $T = 50$ K. (c) Experimental and (d) calculated IXS spectra along the $(HH8)$ r.l.u. direction. The black dots in panels (a) and (c) indicate the positions where IXS spectra were collected.
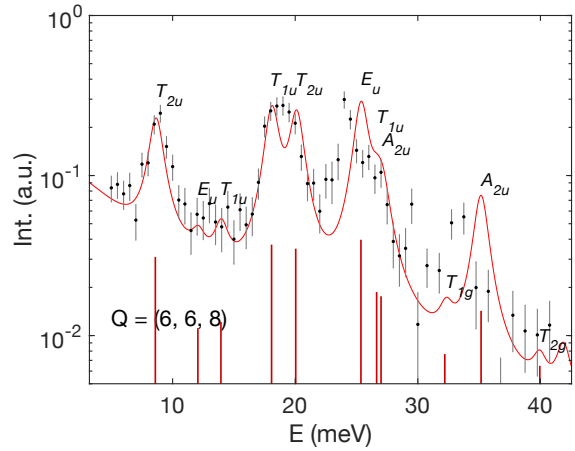

Figure 3. Experimental (black dots) and calculated (red line) phonon spectra at momentum transfer $Q = (6, 6, 8)$ measured at $T = 50$ K. The calculated IXS cross section is convoluted by a pseudo-Voigt instrumental resolution function. The phonon modes corresponding to each peak are indicated, with their calculated energy shown by vertical bars at the bottom. The height of the vertical bars corresponds to the calculated IXS cross sections.

Table 1. Comparison between the experimentally determined and calculated energies of the Raman-active phonon modes for $Eu_2Ir_2O_7$ at room temperature. Energies are measured in units of meV.

	$T_{2g}(1)$	E_g	$T_{2g}(2)$	A_{1g}	$T_{2g}(3)$	$T_{2g}(4)$
experimental [32]	37.5	41.8	47.1	63.0	67.3	84.3
previous cal. [32]	39.3	46.0	51.7	65.7	72.9	83.9
our DFT cal.	39.9	47.2	48.4	66.1	72.9	87.2

Table 2. Comparison between the experimentally determined and calculated energies of the infrared-active T_{1u} phonon modes $Eu_2Ir_2O_7$ at room temperature. Energies are measured in units of meV.

| experimental [32]	14.2	18.5	25.6	42.1	53.8	60.5	78.5
previous cal. [32]	13.9	18.6	27.3	45.4	57.2	61.6	77.6
our DFT cal.	14.0	18.1	26.6	41.9	54.8	64.2	80.0
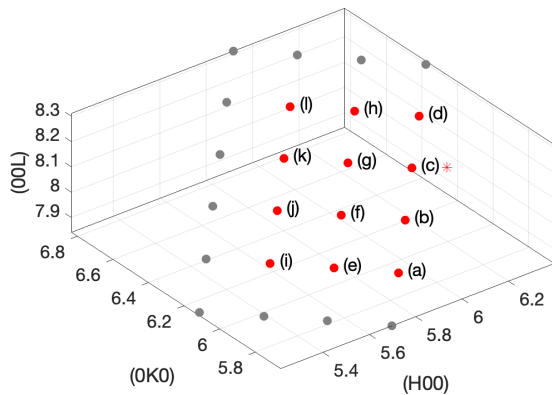
Figure 4. The simultaneously detected 24 Q points in reciprocal space with the targeting detector fixed at $Q = (6.114, 6.088, 8.123)$ r.l.u. as indicated by the asterisk. Red dots correspond to the selected 12 positions that are presented in Fig. 5 and Fig. 6.

directions around (668) in reciprocal space. This area was selected for our IXS measurements due to the relatively low scattering intensity of the acoustic phonon modes. The calculated spectra include convolutions with a pseudo-Voigt function with a full width at half maximum matching that measured form plexiglass from the same analyzer with the same momentum acceptance. While more correctly one should use the full resolution function (e.g. as determined by the method of Ref. [47]), the pseudo-Voigt approximation was considered sufficient for the present work. A comparison between the experimental and calculated cross sections at (668) up to ~ 40 meV is shown in Fig. 3, where the red line is the calculated cross section plus a pseudo-Voigt peak at $E = 0$. The observed phonon modes at the Brillouin zone center can be identified as

the T_{2u} (8.64), E_u (12.08), T_{1u} (13.94), T_{1u} (18.12), T_{2u} (20.10), E_u (25.40), T_{1u} (26.64), A_{2u} (27.13), T_{1g} (32.34), A_{2u} (35.16), and T_{2g} (39.95) modes, where the calculated energies in units of meV are shown in brackets following each mode. The dispersion of the phonon excitations, together with their IXS cross sections, are well described by our DFT calculations.

As the detector bank of the IXS spectrometer at the BL43LXU beamline is composed of 24 detectors that are arranged in a 4-by-6 array, a series of IXS spectra can be collected simultaneously at Q positions around the target wavevector transfer. For a target wavevector transfer of $Q = (6.114, 6.088, 8.123)$ r.l.u., the simultaneously detected Q positions are plotted in Fig. 4, where the target wavevector position is marked by an asterisk.

Figure 5 presents the IXS spectra collected at 12 representative Q positions around (668) measured at $T = 50$ K, below $T_N \sim 115$ K. The Q position for each panel is indicated in Fig. 4 as red dots. The red lines in Fig. 5 represent the calculated cross-sections plus a pseudo-Voigt peak with a FWHM of 1.3 meV at $E = 0$. The experimental data shown in Fig. 5 reveals that in the magnetically ordered phase, the strongest IXS cross section is observed in an energy transfer range of $E \sim [10, 30]$ meV, above which the scattering intensity decreases by an order of magnitude up to $E = 50$ meV. The calculated spectra reproduce the main features of the experimental data, although deviations of ~ 2 meV are observed for the strong modes at 25 and 33 meV. These deviations appear in all detector banks and can be ascribed to the difference in lattice constants employed in our DFT calculations. A second type of deviation is observed at higher energy transfers. For example, at $Q = (6.114, 6.088, 8.123)$ r.l.u. that is close to the Brillouin zone center as shown in Fig. 5(c), a weak peak is observed at ~ 38 meV that
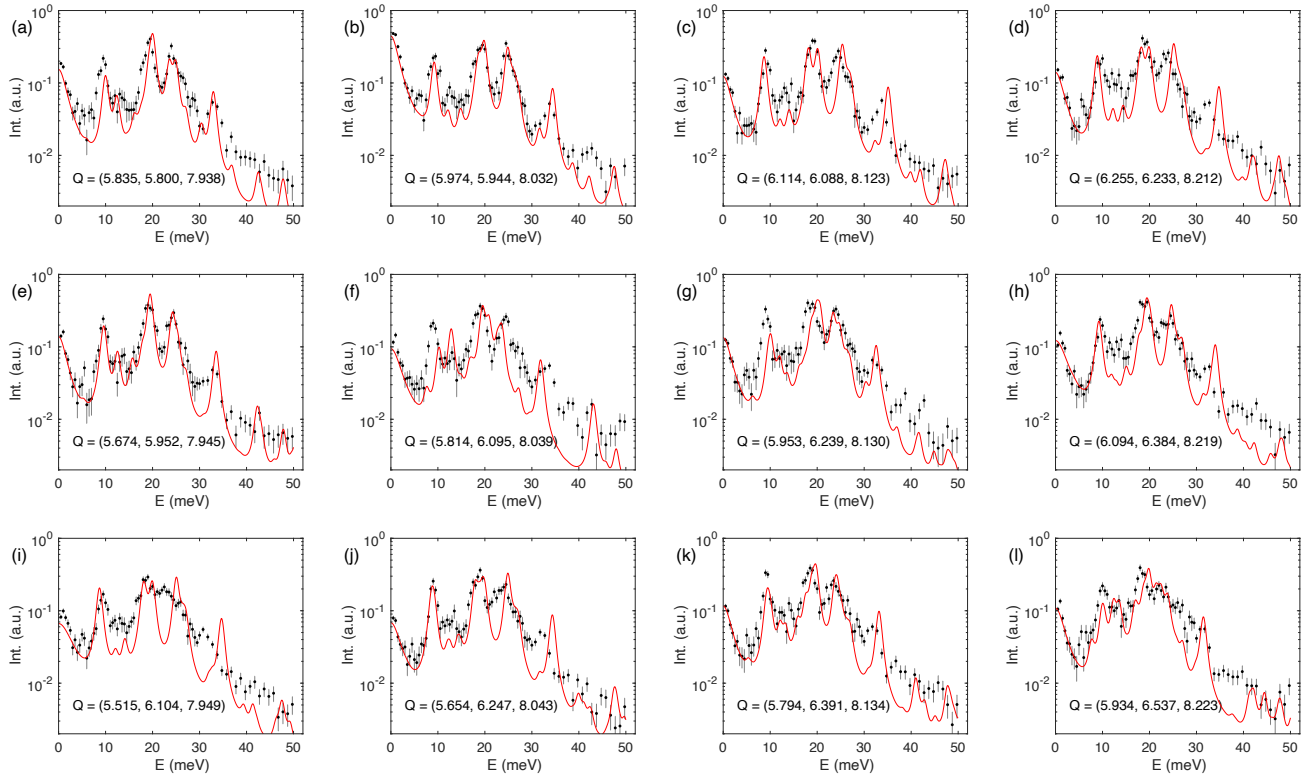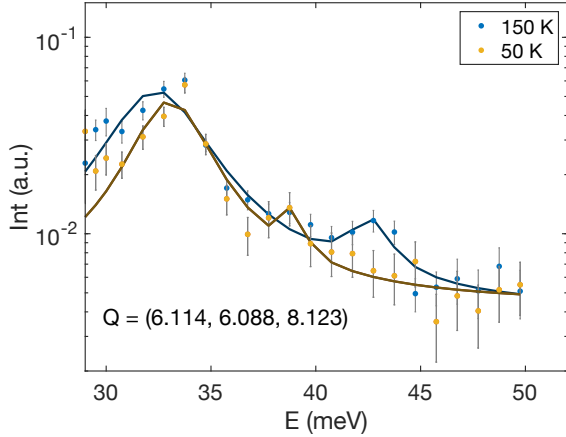
Figure 5. Representative IXS spectra of Eu$_2$Ir$_2$O$_7$ measured at $T = 50$ K with the target detector fixed at $Q = (6.114, 6.088, 8.123)$ r.l.u. Solid red lines represent the calculated phonon cross section convoluted by a pseudo-Voigt instrumental resolution function.
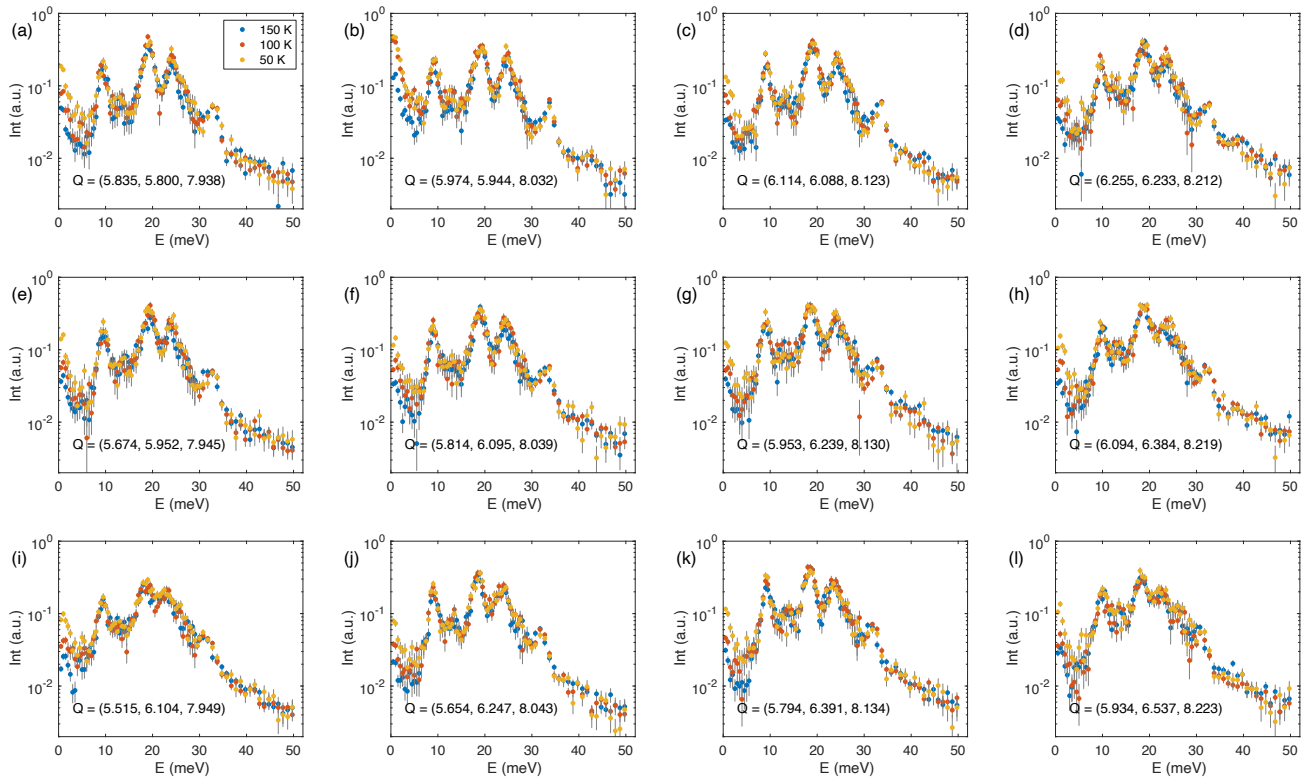
Figure 6. Temperature-dependence of the IXS spectra for Eu$_2$Ir$_2$O$_7$ measured at $T = 50$ K, 100 K, and 150 K.

Figure 7. Comparison of the IXS spectra for $Eu_2Ir_2O_7$ at $Q = (6.114, 6.088, 8.123)$ r.l.u. measured at $T = 150$ (blue) and 50 K (yellow). Solid lines represent fits to the Lorentzian functions and are guide to the eyes.

is not reproduced by the calculation. According to the previous Raman scattering experiments [32], this type of deviation may arise from the softened E_g phonon mode across the magnetic transition temperature $T_N \sim 115$ K.

Figure 6 compares the IXS spectra for the same 12 Q positions at $T = 50$, 100, and 150 K. Focusing at $Q = (6.114, 6.088, 8.123)$ r.l.u., for which the high energy data at $T = 50$ and 150 K is reproduced in Fig. 7, the weak peak observed at $E = 38.8$ meV at $T = 50$ K gradually shifts to $E = 42.8$ meV at $T = 150$ K, which may correspond to the renormalized E_g mode as reported in the previous Raman scattering experiments [32]. Considering the rather weak intensity of the E_g mode, further IXS experiments with better statistics will be required to resolve the dispersion of the E_g mode as a function of momentum transfer and temperature. Besides the mode softening, we also searched for emergent hybridized spin-lattice excitations that were previously observed in Raman scattering experiments [32]. However, the energy of the expected hybridized spin-lattice excitation, which is $\sim$ 26 meV at the Brillouin zone center, overlaps with the strong conventional phonon modes, making it difficult to confirm its existence using our current IXS data. It is also possible that the emergent mode observed at $\sim$ 26 meV in Raman scattering is one of the strong phonon modes that are visible in IXS, which becomes Raman active in the LRO ordered phase.

4. Conclusion

In conclusion, the phonon excitations of the pyrochlore iridate $Eu_2Ir_2O_7$ have been investigated using the non-resonant inelastic x-ray scattering technique.

Comparisons to the DFT calculations reveal that the cross sections are dominated by Raman-inactive modes in an energy transfer range of [10, 30] meV. Analysis of the IXS spectra measured at temperatures below and above T_N reveals possible phonon renormalizations across the long-range-order transition as reported in the previous Raman scattering experiments.

References

[1] Okamoto Y, Nohara M, Aruga-Katori H and Takagi H 2007 *Phys. Rev. lett.* **99** 137207
[2] Balents L 2010 *nature* **464** 199–208
[3] Broholm C, Cava R, Kivelson S, Nocera D, Norman M and Senthil T 2020 *Science* **367** eaay0668
[4] Streltsov S V and Khomskii D I 2016 *Proc. Natl. Acad. Sci. U.S.A.* **113** 10491–10496
[5] Matsuhira K, Wakeshima M, Nakanishi R, Yamada T, Nakamura A, Kawano W, Takagi S and Hinatsu Y 2007 *J. Phys. Soc. Jpn.* **76** 043706
[6] Xu S Y, Belopolski I, Alidoust N, Neupane M, Bian G, Zhang C, Sankar R, Chang G, Yuan Z, Lee C C *et al.* 2015 *Science* **349** 613–617
[7] Pesin D and Balents L 2010 *Nat. Phys.* **6** 376–381
[8] Hasan M Z and Kane C L 2010 *Rev. Mod. Phys.* **82** 3045
[9] Stewart G 2001 *Rev. Mod. Phys.* **73** 797
[10] Prando G, Telang P, Wilson S D, Graf M J and Singh S 2020 *Phys. Rev. B* **101** 174435
[11] Takayama T, Chaloupka J, Smerald A, Khaliullin G and Takagi H 2021 *J. Phys. Soc. Jpn.* **90** 062001
[12] Gardner J S, Gingras M J and Greedan J E 2010 *Rev. Mod. Phys.* **82** 53
[13] Kondo T, Nakayama M, Chen R, Ishikawa J, Moon E G, Yamamoto T, Ota Y, Malaeb W, Kanai H, Nakashima Y *et al.* 2015 *Nat. Commun.* **6** 10042
[14] Lefrançois E, Simonet V, Ballou R, Lhotel E, Hadj-Azzem A, Kodjikian S, Lejay P, Manuel P, Khalyavin D and Chapon L C 2015 *Phys. Rev. Lett.* **114** 247202
[15] Tomiyasu K, Matsuhira K, Iwasa K, Watahiki M, Takagi S, Wakeshima M, Hinatsu Y, Yokoyama M, Ohoyama K and Yamada K 2012 *J. Phys. Soc. Jpn.* **81** 034709
[16] Sagayama H, Uematsu D, Arima T h, Sugimoto K, Ishikawa J, O'farrell E and Nakatsuji S 2013 *Phys. Rev. B* **87** 100403
[17] Disseler S M 2014 *Phys. Rev. B* **89** 140413
[18] Zhao S, Mackie J, MacLaughlin D, Bernal O, Ishikawa J, Ohta Y and Nakatsuji S 2011 *Phys. Rev. B* **83** 180402
[19] Matsuhira K, Wakeshima M, Hinatsu Y and Takagi S 2011 *J. Phys. Soc. Jpn.* **80** 094701
[20] Ueda K, Fujioka J, Takahashi Y, Suzuki T, Ishiwata S, Taguchi Y and Tokura Y 2012 *Phys. Rev. Lett.* **109** 136402
[21] Ueda K, Fujioka J and Tokura Y 2016 *Phys. Rev. B* **93** 245120
[22] Sakata M, Kagayama T, Shimizu K, Matsuhira K, Takagi

S, Wakeshima M and Hinatsu Y 2011 *Phys. Rev. B* **83** 041102

[23] Tafti F, Ishikawa J, McCollam A, Nakatsuji S and Julian S 2012 *Phys. Rev. B* **85** 205104

[24] Ueda K, Fujioka J, Terakura C and Tokura Y 2015 *Phys. Rev. B* **92** 121110

[25] Ueda K, Fujioka J, Yang B J, Shiogai J, Tsukazaki A, Nakamura S, Awaji S, Nagaosa N and Tokura Y 2015 *Phys. Rev. Lett.* **115** 056402

[26] Tian Z, Kohama Y, Tomita T, Ishizuka H, Hsieh T H, Ishikawa J J, Kindo K, Balents L and Nakatsuji S 2016 *Nat. Phys.* **12** 134–138

[27] Ueda K, Oh T, Yang B J, Kaneko R, Fujioka J, Nagaosa N and Tokura Y 2017 *Nat. Commun.* **8** 15515

[28] Ueda K, Kaneko R, Ishizuka H, Fujioka J, Nagaosa N and Tokura Y 2018 *Nat. Commun.* **9** 3032

[29] Wang Y, Weng H, Fu L and Dai X 2017 *Phys. Rev. Lett.* **119** 187203

[30] Imada M, Fujimori A and Tokura Y 1998 *Rev. Mod. Phys.* **70** 1039

[31] Calder S, Vale J G, Bogdanov N, Liu X, Donnerer C, Upton M, Casa D, Said A, Lumsden M, Zhao Z *et al.* 2016 *Nat. Commun.* **7** 11651

[32] Ueda K, Kaneko R, Subedi A, Minola M, Kim B, Fujioka J, Tokura Y and Keimer B 2019 *Phys. Rev. B* **100** 115157

[33] Tóth S, Wehinger B, Rolfs K, Birol T, Stuhr U, Takatsu H, Kimura K, Kimura T, Rønnow H M and Rüegg C 2016 *Nat. Commun.* **7** 13547

[34] Baron A Q 2010 *SPring-8 Inf. Newsl* **15** 14

[35] Baron A Q 2015 *arXiv preprint arXiv:1504.01098*

[36] Baron A Q 2016 *High-Resolution Inelastic X-Ray Scattering I: Context, Spectrometers, Samples, and Superconductors* (Cham: Springer International Publishing) pp 1643–1719 ISBN 978-3-319-14394-1

[37] Millican J N, Macaluso R T, Nakatsuji S, Machida Y, Maeno Y and Chan J Y 2007 *Mater. Res. Bull.* **42** 928–934

[38] Fukui H, Katsura T, Kuribayashi T, Matsuzaki T, Yoneda A, Ito E, Kudoh Y, Tsutsui S and Baron A Q 2008 *J. Synchrotron Radiat.* **15** 618–623

[39] Kresse G and Hafner J 1993 *Phys. Rev. B* **47** 558

[40] Kresse G and Furthmüller J 1996 *Phys. Rev. B* **54**(16) 11169–11186

[41] Blöchl P E 1994 *Phys. Rev. B* **50**(24) 17953–17979

[42] Perdew J P, Burke K and Ernzerhof M 1996 *Phys. Rev. lett.* **77** 3865

[43] Baroni S, Giannozzi P and Testa A 1987 *Phys. Rev. lett.* **58** 1861

[44] Gonze X 1995 *Phys. Rev. A* **52** 1086

[45] Chaput L, Togo A, Tanaka I and Hug G 2011 *Phys. Rev. B* **84** 094302

[46] Togo A and Tanaka I 2015 *Scr. Mater.* **108** 1–5

[47] Ishikawa D and Baron A Q 2021 *J. Synchrotron Radiat.* **28** 804–811